Manipulation of individual superconducting vortices and stick-slip motion in periodic pinning arrays

Xiaoyu Ma, C. J. O. Reichhardt, and C. Reichhardt

Phys. Rev. B **97**, 214521 — Published 25 June 2018

DOI: 10.1103/PhysRevB.97.214521

Individual Superconducting Vortex Manipulation and Stick-Slip Motion in Periodic Pinning Arrays

Xiaoyu Ma[1,2], C. J. O. Reichhardt[1] and C. Reichhardt[1]
[1] *Theoretical Division, Los Alamos National Laboratory, Los Alamos, New Mexico 87545 USA*
[2] *Department of Physics University of Notre Dame, Notre Dame, Indiana 46556 USA*

(Dated: June 13, 2018)

We numerically examine the manipulation of superconducting vortices interacting with a moving trap representing a magnetic force tip translating across a superconducting sample containing a periodic array of pinning sites. As a function of the tip velocity and coupling strength, we find five distinct dynamic phases, including a decoupled regime where the vortices are dragged a short distance within a pinning site, an intermediate coupling regime where vortices in neighboring pinning sites exchange places, an intermediate trapping regime where individual vortices are dragged longer distances and exchange modes of vortices occur in the surrounding pins, an intermittent multiple trapping regime where the trap switches between capturing one or two vortices, and a strong coupling regime in which the trap permanently captures and drags two vortices. In some regimes we observe the counterintuitive behavior that slow moving traps couple less strongly to vortices than faster moving traps; however, the fastest moving traps are generally decoupled. The different phases can be characterized by the distances the vortices are displaced and the force fluctuations exerted on the trap. We find different types of stick-slip motion depending on whether vortices are moving into and out of pinning sites, undergoing exchange, or performing correlated motion induced by vortices outside of the trap. Our results are general to the manipulation of other types of particle-based systems interacting with periodic trap arrays, such as colloidal particles or certain types of frictional systems.

I. INTRODUCTION

Vortices in type-II superconductors interacting with ordered or disordered substrates represent an outstanding example of a condensed matter system with competing interactions, since the vortex-vortex repulsion favors a hexagonal lattice while the substrate ordering can favor different lattice symmetries, leading to commensurate-incommensurate transitions[1–6], depinning phenomena in the presence of an external drive,[7–11], and order-disorder transitions[12–14]. In addition to these basic science issues, vortex motion and pinning are relevant to a variety of applications such as critical current optimization[12,15], while there are a number of proposals for using individual vortex manipulation to test aspects of statistical physics[16,17] or to create new types of vortex logic devices[18–21]. It has also been proposed that vortices in particular materials can support Majorana fermions[22–24], and that individual vortex manipulation and exchange could be used to create certain types of quantum braiding phenomena for quantum computing operations[25,26].

A growing number of experiments have demonstrated individual vortex manipulation using various techniques such as local magnetic fields[27], magnetic force tips[28–32], optical methods[33], local mechanical applied stress[34], nanoscale electrostatic manipulation[35], local applied currents[36], and tunneling microscope tips[37,38]. Numerous related works describe the dynamics of individually manipulated or dragged colloidal particles moving through glassy[39–43] or crystalline systems[44,45], where the fluctuations of the probe particle can be used to induce local melting or to study changes in the viscosity across an order-disorder transition. Understanding the different kinds of dynamics associated with particle manipulation on periodic substrates is relevant for vortices in superconductors[1,46] or Bose-Einstein condensates[47], as well as for other particle based systems with periodic substrates such as skyrmions[48], ions on optical traps[49], colloidal particles[50–52], and nanofriction systems where individual atoms or molecules can be dragged with a tip[53]. In many of the previous numerical works on the local manipulation of dragged particles, the trap used for manipulation is strong enough to permanently bind a single particle and drag it under a constant force. A more accurate model of recent experiments on vortices in a type-II superconductor is a trap of fixed strength moving at fixed velocity that can couple to or decouple from an individual vortex. Vortices dragged by such a trap can either move at the average velocity of the trap or decouple and fall away from the trap, and the trapping of multiple vortices is also possible.

Here we consider a trap with a finite confining force or strength moving across a superconductor containing a periodic array of pinning sites. As a function of trap strength and velocity we identify five generic dynamic phases and several subphases. At low coupling or high trap velocities we find a decoupled phase (I) where the trap can only shift a vortex within a pinning site but cannot depin the vortex. For larger coupling or smaller tip velocities, there is an intermediate coupling phase (II) where a single vortex can be dragged out of the pinning site but is trapped by the next pinning site it encounters in an exchange process. In the intermediate trapping phase (III), vortices can be dragged over a distance of several lattice constants and additional vortex exchange modes arise in adjacent pinning sites. For stronger coupling, there is an intermittent multiple trapping phase (IV) in which the trap alternates between capturing one and two vortices, producing telegraph noise in the trap force fluctuations. At the strongest coupling and lowest trap velocities we find a strong coupling phase (V) where the trap permanently captures two vortices. These phases are associated with distinct signatures in the force fluctuations exerted on the moving trap, such as stick-slip signals produced when vortices exit and enter pinning sites or exchange positions in the trap. We observe nonmonotonic behavior in which the trapping effectiveness increases as the trap velocity decreases, but for the highest trap velocities the system is always in a decoupled phase. We map the dynamic phases as a function of coupling strength, trap velocity, and the angle between the driving direction and the pinning lattice symmetry direction. We also study the effect on the behavior of changing the shape of the pinning sites.

Our results should also be relevant to other types of particle assemblies driven over periodic substrates. One example of such a system is colloids on periodic substrates[11,50–52], where a single colloid can be dragged with an optical trap at different angles with respect to the substrate symmetry directions. Similar dragging techniques could be used for skyrmions[48] or ions on periodic substrates[49]. We specifically focus on modeling effectively two-dimensional vortices, which can represent either bulk samples containing very stiff vortex lines or thin film samples. For three-dimensional vortices that are not stiff or for layered superconductors, additional effects that we do not model can occur, such as bending of the vortex lines or decoupling of vortex segments between the layers.

II. SIMULATION AND SYSTEM

We consider a two-dimensional system with periodic boundary conditions in the x and y-directions containing N_v vortices modeled as point particles interacting with a square periodic pinning array. We work in two dimensions since this is much more numerically tractable than a fully three-dimensional simulation, and more importantly, many of the related systems mentioned above can appropriately be studied in the two-dimensional limit. The magnetic field applied perpendicular to the sample plane is set to the matching field $B = B_\phi$ at which the number of vortices equals the number of pinning sites. We introduce a trap of radius R_{tr} that moves across the sample, representing a magnetic force microscope (MFM) tip as illustrated schematically in Fig. 1(a). The MFM tip creates a localized potential with a finite trapping force that can capture one or more vortices, and it travels at a constant velocity V_{tr} at an angle θ with respect to the x-axis symmetry direction of the pinning lattice. The dynamics of vortex i are determined by the overdamped

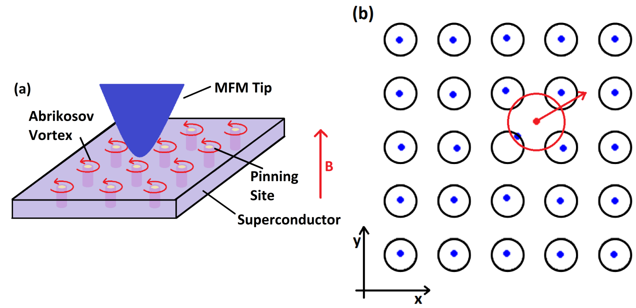

FIG. 1: (a) Schematic of a superconducting slab containing a square array of artificial pinning sites (yellow) occupied by vortices (red arrows). The number of vortices produced by the magnetic field $\mathbf{B}$ applied perpendicular to the sample plane matches the number of pinning sites. A magnetic force microscope (MFM) tip moves over the sample surface at velocity v_{tr} and is represented by a finite range harmonic trap with a trapping force or strength that can be varied by adjusting the distance between the MFM tip and the sample. (b) Schematic of a $5\lambda \times 5\lambda$ subsection of the system. Open black circles are pinning sites, filled blue circles are the vortices, and the large red circle is the trap which is moving at an angle of $\theta = 30^\circ$ relative to the x axis symmetry direction of the pinning array as indicated by the red arrow.

equation of motion

$$\eta \frac{d\mathbf{r}_i}{dt} = \mathbf{F}_i^{vv} + \mathbf{F}_i^{vp} + \mathbf{F}_i^{tr}. \tag{1}$$

Here $\mathbf{r}_i$ is the position of vortex i and we set the damping coefficient $\eta = 1$. All forces are measured in units of $f_0 = \phi_0^2/(2\pi\mu_o\lambda^3)$ where $\phi_0 = h/2e$ is the flux quantum and λ is the London penetration depth. The first term on the right hand side describes the repulsive vortex-vortex interactions, $\mathbf{F}_i^{vv} = \sum_{j=1}^{N_v} K_1(r_{ij})\hat{\mathbf{r}}_{ij}$, where $r_{ij} = |\mathbf{r}_i - \mathbf{r}_j|$, $\hat{\mathbf{r}}_{ij} = (\mathbf{r}_i - \mathbf{r}_j)/r_{ij}$, and K_1 is the modified Bessel function of the second kind. The pinning forces arise from a square lattice of finite range harmonic wells, $\mathbf{F}_i^{vp} = -\sum_{k=1}^{N_p}(F_p/r_p)(\mathbf{r}_i - \mathbf{r}_k^{(p)})\Theta(r_p - |\mathbf{r}_i - \mathbf{r}_k^{(p)}|)$, where $F_p = 0.3$ is the maximum pinning force, $r_p = 0.3$ is the pin radius, $\mathbf{r}_k^{(p)}$ is the location of the k-th pinning site, and Θ is the Heaviside step function. The force from the moving trap $\mathbf{F}_i^{tr}$ has the same form as the pinning interaction but with a maximum trapping force of F_{tr} and a trapping radius $R_{tr} = 0.5$. The trap translates at a constant velocity of v_{tr}.

We consider a 20×20 square pinning array at a field of $B/B_\phi = 1.0$, where B_ϕ is the matching field at which there is one vortex per pinning site. The pinning lattice constant is $a = 1.0$ and we measure all distances in terms of λ. We initialize the system with each pinning site occupied by a vortex. Figure 1(b) schematically illustrates a 5×5 subsection of the sample showing the motion of the trap, which is dragging a single vortex. We measure the vortex displacements in and outside of the trap as well as the time series of the force fluctuations on the moving trap. During an individual run we translate the trap a total distance of $D_x = 300a$ in the x direction, corresponding to a total distance of $D_x/\cos(\theta)$ in the driving direction. Throughout this work we describe distances in terms of their projections into the x direction.

We define the time and location at which an individual vortex i becomes captured by the trap as $(t^i_{in}, \mathbf{r}^i_{in})$, and the corresponding time and location at which vortex i escapes from the trap as $(t^i_{out}, \mathbf{r}^i_{out})$. We can then write the individual capture length $C^i_l = |\mathbf{r}^i_{out} - \mathbf{r}^i_{in}|\cos(\theta)/a$ as a measure of the distance vortex i travels inside the trap projected into the x direction and normalized by the pinning lattice constant a. This measure indicates how far a given vortex is dragged. For example, if a trap moving in the x direction captures a vortex and drags it over a distance $|\mathbf{r}^i_{out} - \mathbf{r}^i_{in}| = 100a$, then $C^i_l = 100$. If instead the trap only drags the vortex from one pinning site to the next, $C^i_l \approx 1.0$. We define the average capture length as $C_l = N_c^{-1}\sum_{i=1}^{N_v} C^i_l$, where N_c is the total number of vortices captured by the trap during the measurement interval.

The initial conditions we consider, with the vortices initially trapped in the pinning sites, corresponds to a field cooled sample. If the field were applied to a sample that is already superconducting, vortices would enter from the edges and the vortex configuration would be more disordered. We choose a square pinning array since such arrays have already been experimentally realized. The symmetry of the square array makes it easier to understand the results for driving at different angles with respect to the principal symmetry directions of the array. Our results should be robust for triangular pinning arrays; however, the detailed dependence on the angle of driving would be different.

III. RESULTS

We first consider a system with a trap of strength $F_{tr} = 1.0$ moving at an angle of $\theta = 30^\circ$ with respect to the x axis of the pinning array. In Fig. 2(a) we show the vortex and pinning site locations along with the trajectories of the vortices and the trap over a fixed period of time in the decoupled phase I at a trap velocity of $v_{tr} = 0.5$. Vortices in the pinning sites wiggle a small amount as the trap passes over them but they do not depin. For $0.19 < v_{tr} < 0.375$, we find an intermediate coupling phase II in which the trap captures a vortex and drags it a projected distance of approximately $2a$ to the next pinning site along the trap trajectory, where the trapped vortex exchanges places with the pinned vortex. In Fig. 2(b), the vortex trajectories in phase II at $v_{tr} = 0.2$ extend from pin to pin following the motion of the trap. For $v_{tr} < 0.19$ we find an intermediate trapping phase III where individual vortices remain inside the trap for distances greater than $2a$ but are not permanently trapped. Simultaneously, vortex exchange motions emerge in the surrounding pinning sites, as illustrated in Fig. 2(c) for $v_{tr} = 0.02$.

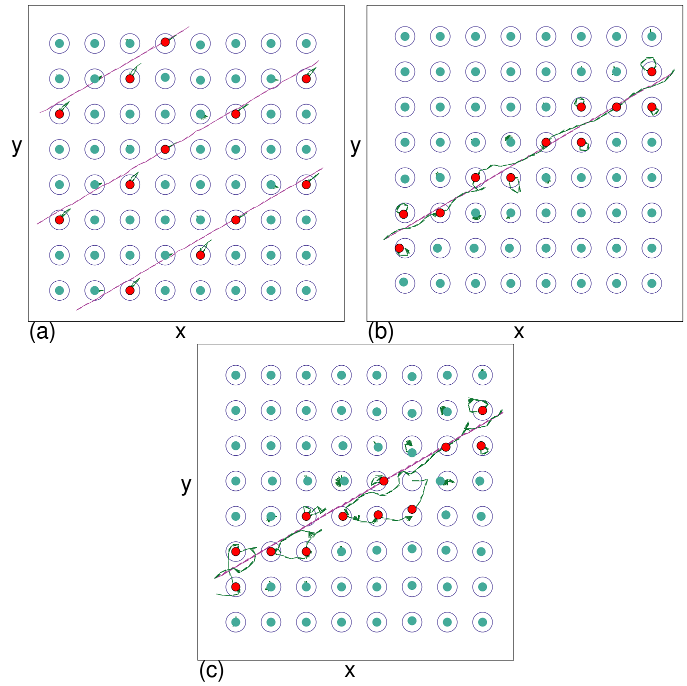

FIG. 2: Vortex positions (filled circles), pinning site locations (open circles), tip trajectory (magenta line), and vortex trajectories (green lines) in an $8\lambda \times 8\lambda$ portion of a system with $F_{tr} = 1.0$ and $F_p = 0.3$ where the trap moves at an angle of $\theta = 30^\circ$ with respect to the x axis of the pinning array. Red filled circles indicate vortices that were displaced a distance of at least a pin radius due to the motion of the trap. (a) The decoupled phase I at $v_{tr} = 0.5$, marked A in Fig. 3(a), where all the vortices remain pinned. (b) The intermediate couping phase II at $v_{tr} = 0.2$, marked B in Fig. 3(a), where individual vortices travel a distance $2a$ with the trap before escaping and being replaced by a new trapped vortex. (c) The intermediate trapping phase III at $v_{tr} = 0.02$, marked C in Fig. 3(a), where in addition to translations of the trapped vortex, vortices near but outside the trap move in exchange rings through neighboring pinning sites.

The effect of the trap on individual vortices is illustrated in Fig. 3(a), where we plot the capture length C_l versus the trap velocity v_{tr} for a trap with $F_{tr} = 1.0$ and $\theta = 30^\circ$. We observe a clear drop in C_l for $v_{tr} > 0.375$ when the system enters the decoupled phase I in which the trap moves too rapidly to capture any of the pinned vortices. In phase I, $C_l \ll 1.0$ but it remains nonzero since the trap drags individual vortices a small distance within the pinning site. We find that there is an optimal trapping velocity $v_{tr} = 0.012$ corresponding to the peak in C_l where the vortex can on average be trapped for distances as large as $18a$ before exchanging places with a pinned vortex. For $v_{tr} < 0.012$, C_l drops dramatically when the trap velocity becomes so slow that vortices have enough time to escape from the trap or exchange with neighboring pinned vortices. The escape of the vortices is purely a dynamical effect since we are working in the regime of no thermal fluctuations. In contrast,

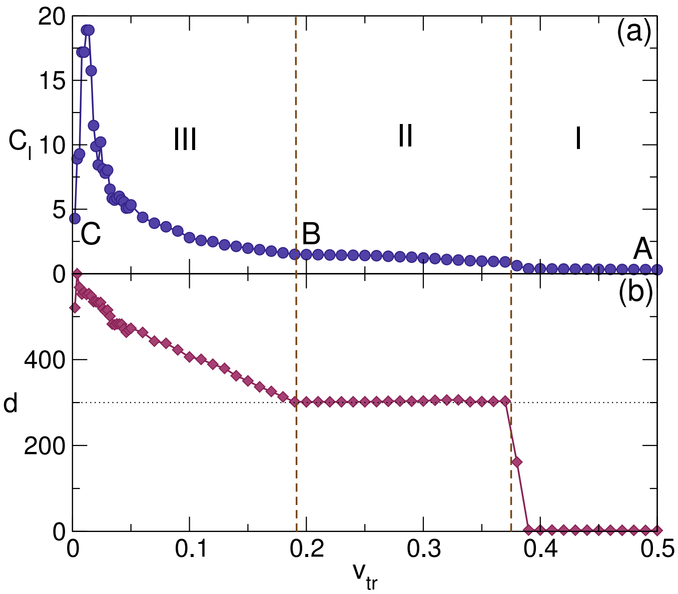

FIG. 3: (a) Capture length C_l, the average distance a vortex is dragged by the trap, vs trap velocity v_{tr} in the system from Fig. 2 with $F_{tr} = 1.0$ and $\theta = 30^\circ$. The points marked A, B, and C correspond to v_{tr} values at which the images in Fig. 2 were obtained. (b) The total displacements d of all the vortices over a time interval during which the trap translates by $D_x = 300a$ vs v_{tr}. Above $v_{tr} = 0.375$, we find the decoupled phase I in which the trap does not drag any vortices. In the intermediate coupling phase II for $0.19 < v_{tr} < 0.375$, an individual vortex can be dragged by the trap a distance of $2a$ before exchanging places with a pinned vortex. For $v_{tr} < 0.19$, the system is in the intermediate trapping phase III where vortices can be dragged a distance of several lattice constants and additional vortices exchange positions among the sites close to the trap. For $v_{tr} < 0.012$, vortices are able to escape more easily from the slow trap so C_l drops while d remains large.

for $v_{tr} > 0.012$, the trapped vortex can remain trapped since it does not have enough time to exchange with another vortex. As v_{tr} increases above 0.012, C_l drops as the trapped vortex experiences larger displacements until the system reaches the II-III transition where the trapped vortex always exchanges with a pinned vortex.

To measure the global effect of the trap, in Fig. 3(b) we plot the scaled net total projected displacement d of all the vortices $d = a^{-1}\sum_{i=0}^{N_v} |(\mathbf{r}^i(t_0+\tau) - \mathbf{r}^i(t_0)) \cdot \hat{\mathbf{x}}|$ versus v_{tr}, where $\tau = D/(v_{tr}\cos(\theta))$ is the time required for the trap to translate a projected distance of $D = 300a$. We start the measurement at time $t_0 \neq 0$ since we wait for a period of time before beginning the measurement in order to avoid transient effects. Above the I-II transition at $v_{tr} = 0.375$, d drops to zero. In the intermediate coupling phase II, the trap is never empty, and there is a plateau with $d = 300$ throughout the phase II region of $0.19 < v_{tr} < 0.375$. No individual vortex travels this distance with the trap; instead, as shown in Fig. 3(a), vortices translate an average distance of $C_l = 2a$ before encountering a pinning site and exchanging with the pinned vortex. The surrounding vortices remain pinned and do not contribute to d. In the intermediate trapping phase III for $v_{tr} < 0.19$, d increases with decreasing v_{tr} as vortices surrounding the trap begin to depin from the pinning sites and undergo rotational exchange motions of the type illustrated in Fig. 2(c) at $v_{tr} = 0.02$.

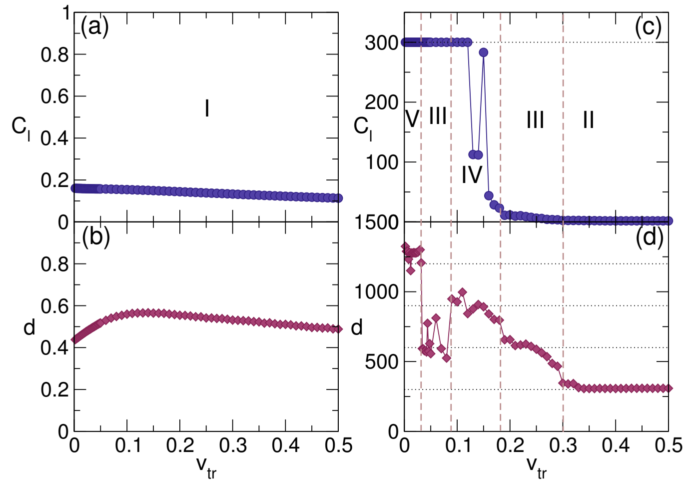

FIG. 4: (a) C_l vs v_{tr} and (b) d vs v_{tr} for the $\theta = 30^\circ$ system with a decreased trap strength of $F_{tr} = 0.5$. The motion is always in the decoupled phase I. (c) C_l vs v_{tr} and (d) d vs v_{tr} in the same system for a strong trap with $F_{tr} = 1.8$, where dashed lines indicate the boundaries of phases II, III, IV, and V. In the intermittent multiple trapping phase IV, the trap intermittently captures two vortices, and in the strongly coupled phase V, the trap always captures two vortices. A reentrant window of phase III appears just above phase V.

We find transitions among the different phases as a function of trap strength F_{tr} as well as trap velocity. Figure 4(a,b) shows C_l and d versus v_{tr} for driving at $\theta = 30^\circ$ in the same system from Fig. 3 with a smaller $F_{tr} = 0.5$. Both C_l and d are less than one, and the system remains in the decoupled phase I for all values of v_{tr}. In Fig. 4(c,d), we find that additional phases appear when the trap strength is increased to $F_{tr} = 1.8$. These include phase IV, where the trap alternates between capturing one and two vortices, and phase V, where the trap always captures two vortices. Here phase II appears for $v_{tr} > 0.3$, while for $v_{tr} < 0.03$ the system is in phase V and the trap always contains two vortices. There is a reentrant window of phase III just above phase V.

In Fig. 5(a) we illustrate the vortex trajectories in phase V at $v_{tr} = 0.02$, where a multi-vortex exchange process occurs in the vortices adjacent to the trap. The two trapped vortices produce a repulsion that is strong enough to depin the vortex in the pin traversed by the trap along with those in a pair of neighboring pins on either side of the trap. The three depinned vortices form a cascading loop of reoccupancy, and one of them moves to occupy the pinning site behind the trap that was previously vacated. For $0.03 < v_{tr} < 0.1$ and

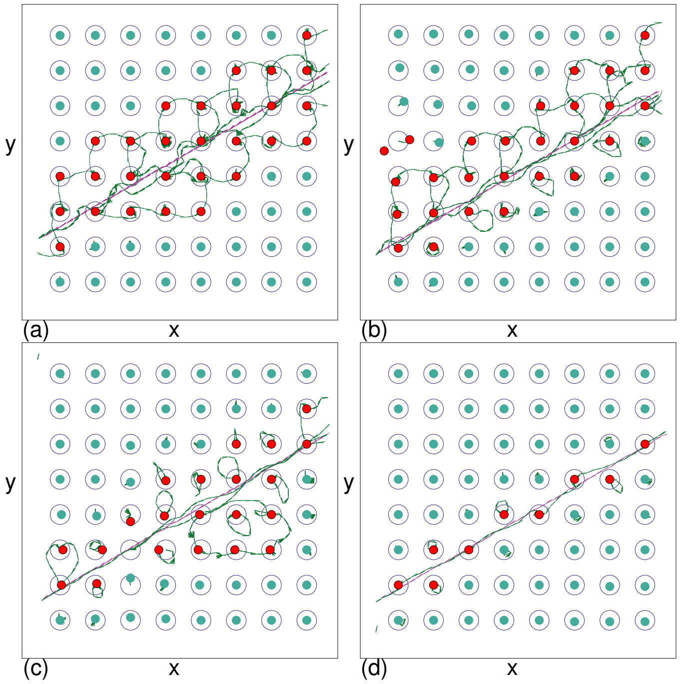

FIG. 5: Vortex positions (filled circles), pinning site locations (open circles), tip trajectory (magenta line), and vortex trajectories (green lines) in an $8\lambda \times 8\lambda$ portion of the $F_{tr} = 1.8$ system in Fig. 4(c,d). Red filled circles indicate vortices that were displaced a distance of at least a pin radius due to the motion of the trap. (a) At $v_{tr} = 0.02$ in phase V, the trap always contains two vortices and correlated ringlike exchanges of vortices occur in the surrounding regions. As the trap moves, the two trapped vortices dislodge three pinned vortices, and one of these vortices jumps into the empty pinning site immediately behind the moving trap. (b) At $v_{tr} = 0.12$ in phase IV, the trap alternates between capturing one and two vortices. (c) Disordered flow in phase III at $v_{tr} = 0.25$, with a much weaker perturbation of the surrounding pinned vortices. (d) At $v_{tr} = 0.5$ in phase II, a vortex only travels a short distance with the trap before exchanging with a pinned vortex.

$0.018 < v_{tr} < 0.3$ we find the intermediate trapping phase III, while for $0.1 < v_{tr} < 0.018$, an intermittent multiple trapping phase IV occurs in which the trap alternates between capturing one or two vortices. Figures 5(b) and (c) illustrate typical phase IV and phase III trajectories, respectively. Phase IV contains several subregimes. When v_{tr} is close to 0.1, the trap permanently captures one vortex and exchanges a second vortex with each pinning site it passes, while at larger v_{tr}, both trapped vortices exchange places with vortices in the pinning sites as the trap moves. We note that simulations using a Landau-Ginzburg approach have shown that sufficiency strong pinning sites can simultaneously capture two vortices[54]. In our case the multiply occupied pinning site takes the form of a moving trap, but multi-vortex trapping by pinning sites has been demonstrated as feasible in more realistic models that operate beyond the London limit[54].

In Fig. 6(a) we plot a heat map of the total displacements d as a function of trap strength F_{tr} versus trap velocity v_{tr} for a driving angle of $\theta = 30^\circ$ in which we highlight the locations of phases I through V. For $F_{tr} < 0.75$, the system is in the decoupled phase I. The effect of changing the angle of drive on d appears in the F_{tr} versus v_{tr} heat maps in Fig. 6(b,c,d) for $\theta = 0^\circ$, 15°, and 45°, which trace the evolution of the five different phases. In each case, the transition lines generally shift to higher values of F_{tr} with increasing v_{tr}. For $\theta = 0^\circ$ in Fig. 6(b), the trap does not start dragging vortices out of the pinning sites until $F_{tr} > 1.25$, and we observe a variety of additional subphases that are not present at larger θ. The subphases are variations of phases V and IV in which either two vortices are captured by the trap or two vortices are exchanged in a variety of distinct orbits which produce various jumps and dips in d and C_l, as seen near $F_{tr} = 0.18$ and $v_{tr} < 0.1$. Previous work for vortices driven over square periodic pinning arrays at $\theta = 0^\circ$ showed a series of distinct dynamical phases associated with positive or negative jumps in the velocity-force curves[8,9,55,56], and the dynamics we observe in Fig. 6(b) is consistent with this type of behavior. In the $\theta = 15^\circ$ phase diagram of Fig. 6(c), there is less jumping between phases V and IV for $F_{tr} > 1.6$, and there is an extended region of phase II flow. At $\theta = 45^\circ$ in Fig. 6(d), the region containing phase V is smaller but we find the same general phase behavior as described above for other values of θ.

In Fig. 7(a) we plot d versus v_{tr} for the $\theta = 0^\circ$ sample at $F_{tr} = 1.8$, where we find numerous jumps at small v_{tr}. In contrast, the plot of d versus v_{tr} in Fig. 7(b) at $F_{tr} = 1.8$ and $\theta = 45^\circ$ has a smoother behavior at small v_{tr} and a step marking the II-III transition at $v_{tr} = 0.25$.

The transition between a trap that can drag a vortex and a trap that cannot drag a vortex is similar to the transition from weak to strong pinning near a Labusch point[57]. In our system, in the absence of pinning a single trap can always drag a vortex, and if the vortices are strongly coupled with each other, the single trap would drag the entire vortex assembly which would act like an elastic solid. When pinning is present that is strong enough to hold back the vortex motion, there is a transition point at which the vortex assembly decouples from the moving trap. There have been several observations of vortex decoupling transitions produced when a dragged portion of the vortex assembly decouples from the remainder of the assembly, including the driving of vortices coupled to magnetic degrees of freedom in magnetic superconductors[58], the dissociation of composite vortices in multi-component superconductors[59], decoupling of vortices in layered systems[60], and driven transitions of vortices to a phase slip regime[61].

In Fig. 8(a) we show the vortex and trap trajectories in phase II for a sample with $F_{tr} = 1.8$ and $\theta = 0^\circ$ at $v_{tr} = 0.35$. Individual vortices are trapped over a distance of one lattice constant, moving along a one-dimensional path defined by the trap trajectory and in-

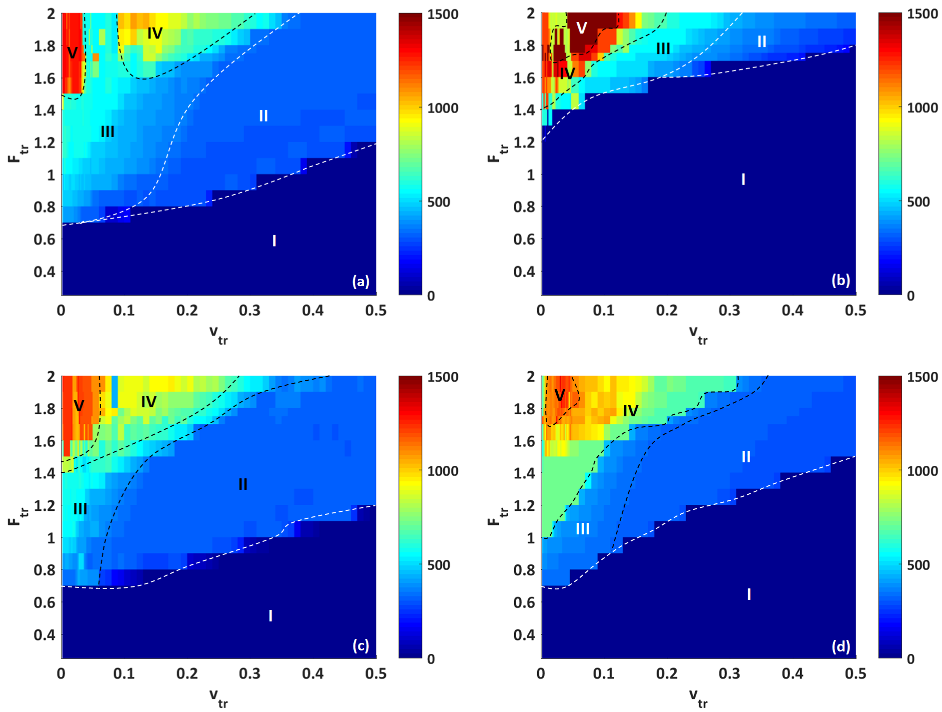

FIG. 6: Heat map of the total displacements d as a function of F_{tr} vs v_{tr} for driving at (a) $\theta = 30°$, (b) $\theta = 0°$, (c) $\theta = 15°$, and (d) $\theta = 45°$. Dashed lines are guides to the eye indicating the locations of the different phases: I (decoupled), II (intermediate coupling), III (intermediate trapping), IV (intermittent multiple trapping) and V (strongly coupled).

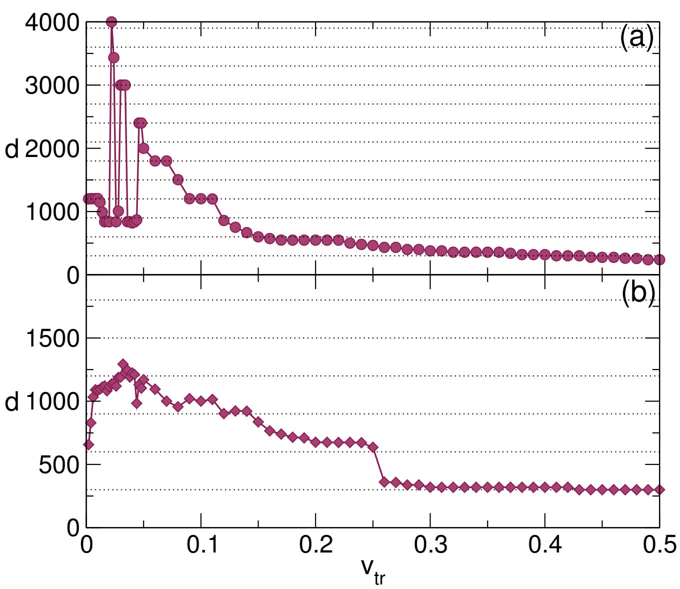

FIG. 7: d vs v_{tr} at $F_{tr} = 1.8$. Dashed lines indicate intervals corresponding to the distance $300a$ traveled by the trap during the simulation. (a) At $\theta = 0°$, there is no II-I transition, but the jumps in d for $v_{tr} < 0.075$ indicate the location of the V-IV transition, while the drop in d near $v_{tr} = 0.1125$ corresponds to the IV-III transition. (b) At $\theta = 45°$, a clear drop in d occurs at the IV-III transition near $v_{tr} = 0.25$. Another drop in d appears at small v_{tr} where the system is in region IV but jumps to region V as the trap velocity increases.

ducing few to no perturbations in the surrounding vortices before exchanging positions with the next pinned vortex along the path of the trap. At $v_{tr} = 0.1$ in Fig. 8(b), the perturbations to the surrounding vortices are stronger, while at $v_{tr} = 0.02$ in Fig. 8(c), there is continuous plastic mixing of the vortices in the two rows of pins on either side of the trap trajectory. For driving along $\theta = 45°$, Fig. 8(d) shows that in phase II at $F_{tr} = 1.8$ and $v_{tr} = 0.35$, motion occurs along the diagonal with some distortions of the vortices in the adjacent pinning sites.

IV. EFFECT OF PINNING POTENTIAL SHAPE

In Sec. III we employed parabolic pinning sites with an attractive force that is cut off beyond the pinning radius. Since there are many different ways to create pinning sites, an important question is how the results change for different forms of the pinning potential. The most generic variation of the pinning is to introduce a smooth cutoff of the pinning force. To address this, we change the form of the pinning potential to a Gaussian shape, $U(r) = U_p \exp(-\kappa R^2)$. We set $U_p = 0.045$ and $\kappa = 50$ to obtain $\mathbf{F}_i^{vp} = -\sum_{k=1}^{N_p} 2\kappa U_p \exp[-\kappa(\mathbf{r}_i - \mathbf{r}_k^{(p)})^2](\mathbf{r}_i - \mathbf{r}_k^{(p)})$. In Fig. 9(a) we plot the shapes of the Gaussian and parabolic pinning potentials, and in Fig. 9(b) we show the resulting pinning forces. We choose the parameters of the Gaussian potential such that both types of poten-

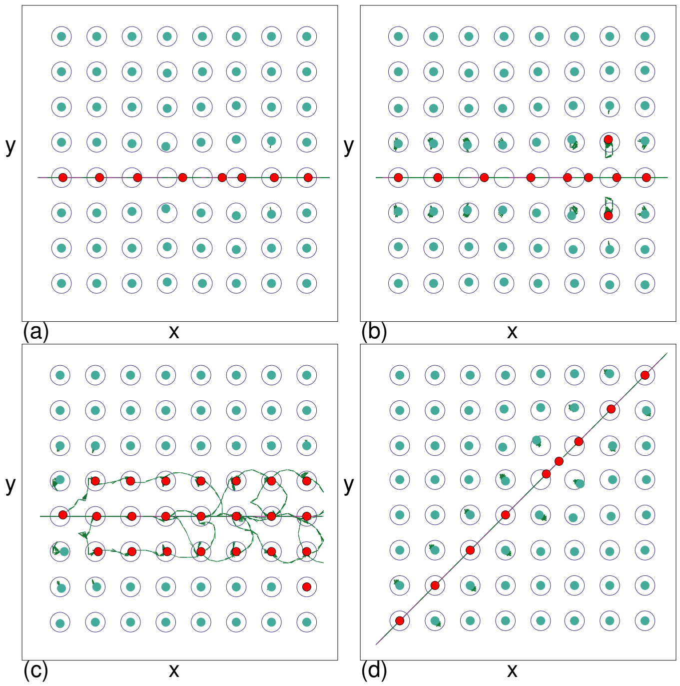

FIG. 8: Vortex positions (filled circles), pinning site locations (open circles), tip trajectory (magenta line), and vortex trajectories (green lines) in an $8\lambda \times 8\lambda$ portion of a sample with $F_{tr} = 1.8$ and (a-c) $\theta = 0°$. (a) Phase II at $v_{tr} = 0.35$, where there is little distortion of the background. (b) Phase III at $v_{tr} = 0.1$, where the amount of distortion of the surrounding vortices has increased. (c) Phase IV at $v_{tr} = 0.02$, where the multiple dragged vortices induce plastic motion in the surrounding vortices. (d) The phase II motion at $v_{tr} = 0.35$ in a sample with $\theta = 45°$.

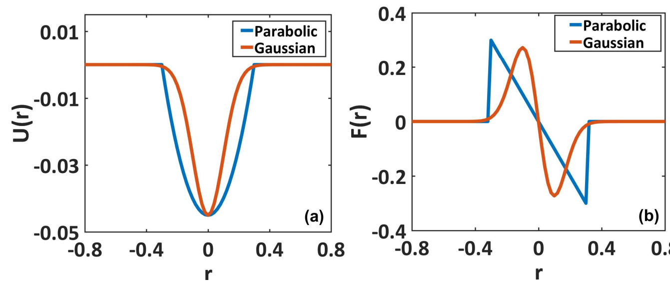

FIG. 9: (a) The shape $U(r)$ of the pinning potential for parabolic (blue) and Gaussian (red) pinning sites. (b) The corresponding pinning force $F_p(r)$ showing a sharp cutoff for the parabolic pins and a smooth cutoff for the Gaussian pins.

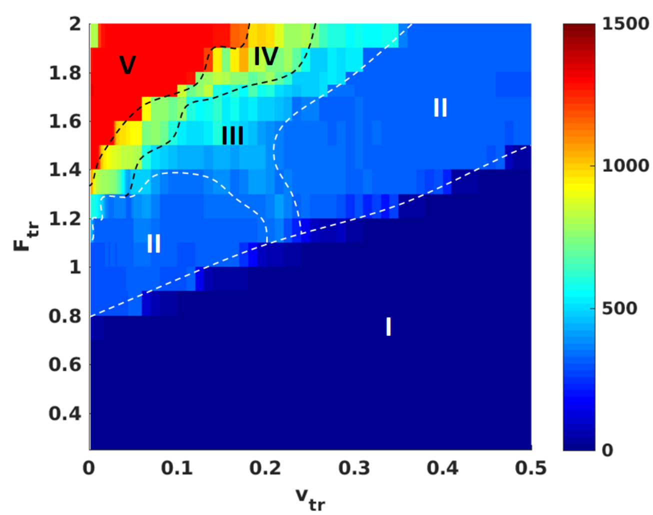

FIG. 10: Heat map of the total displacements d as a function of F_{tr} vs v_{tr} for the system in Fig. 6(a) with driving at $\theta = 30°$ where the parabolic pinning has been replaced by Gaussian pinning. Dashed lines are guides to the eye indicating the locations of the different phases: I (decoupled), II (intermediate coupling), III (intermediate trapping), IV (intermittent multiple trapping), and V (strongly coupled). Compared to Fig. 6(a), some small changes in the locations of phases I to V appear, but both the smooth and the parabolic pinning sites exhibit the same dynamic phases.

tial produce the same maximum pinning force. We map the dynamic phase diagram as a function of F_{tr} vs v_{tr} for the Gaussian pinning potential in Fig. 10 with driving at $\theta = 30°$, where the same dynamic phases found in Fig. 6(a) for parabolic pinning appear. The I-II transition has the same general features for both types of pinning, occurring at similar values of F_{tr} in each case and shifting to higher values of F_{tr} as v_{tr} increases. The window of phase V at small v_{tr} and large F_{tr} is larger for Gaussian pinning than for parabolic pinning, while phase IV covers a smaller area for the Gaussian pinning. The results in Fig. 10 indicate that phases I through V robustly appear for different pinning potentials. We note that while all the phases reported for the parabolic pinning also arise with the Gaussian pinning, there are some differences in the phase diagram. In particular, phases IV and V are expanded for the Gaussian pinning, while phases I and II are very similar for each type of pinning.

V. FORCE FLUCTUATIONS

We next examine the time series of the x direction forces f_x experienced by the trap as it moves in the different phases. In Fig. 11(a) we plot a representative time series of f_x for the $\theta = 30°$ system from Fig. 2(a) and Fig. 3(a) in the decoupled phase I at $F_{tr} = 1.0$ and $v_{tr} = 0.5$. We find a pronounced stick-slip character in f_x with a strong asymmetry of sudden increases and gradual decreases. The slow drops in f_x occur when the moving trap is dragging a vortex inside a pinning site and the force from the pinning site is resisting the pull of the trap, while the rapid increases correspond to intervals

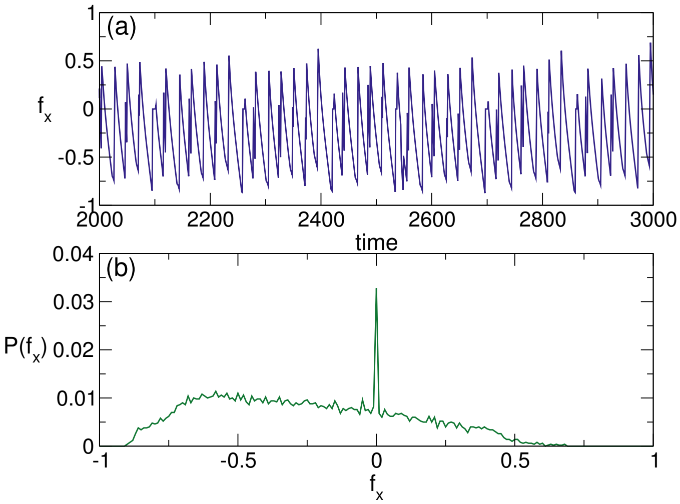

FIG. 11: (a) A representative plot of the time series of the x direction forces f_x experienced by the moving trap in phase I at $\theta = 30°$, $F_{tr} = 1.0$, and $v_{tr} = 0.5$. (b) The corresponding distribution function $P(f_x)$. The time intervals when the trap does not contain a vortex produce the peak at $f_x = 0$.

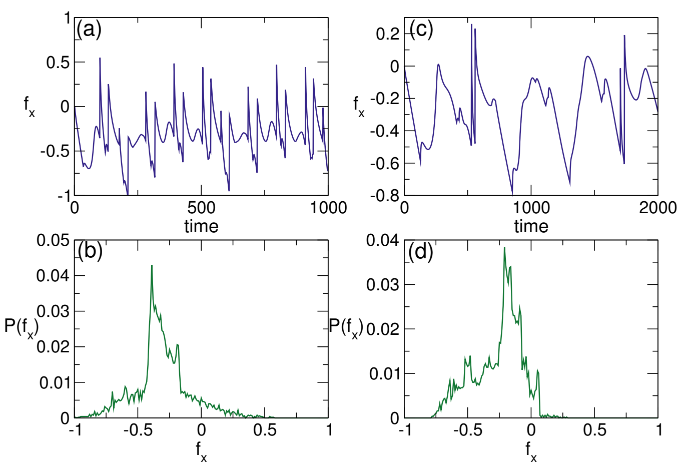

FIG. 12: (a) A representative segment of $f_x(t)$ in phase II at $v_{tr} = 0.2$ for a sample with $\theta = 30°$ and $F_{tr} = 1.0$. (b) The corresponding $P(f_x)$. There is no peak at $f_x = 0$ since the trap always contains a vortex. (c) $f_x(t)$ in the same sample in phase III at $v_{tr} = 0.05$. (d) The corresponding $P(f_x)$ contains additional peaks produced by additional modes of motion.

when the vortex decouples from the trap and drops back into the pinning site. Figure 11(b) shows that the probability distribution function $P(f_x)$ has a spike at $f_x = 0$ produced by the time periods during which there is no vortex inside the trap. There is a local maximum in $P(f_x)$ near $f_x \approx -0.6$, the value of the x component of the average decoupling force $F_{\rm dc}$ at which the vortex escapes from the trap and is pushed back into the pinning site by the restoring force from the surrounding pinned vortices.

In Fig. 12(a,b) we plot $f_x(t)$ and $P(f_x)$ in phase II at $v_{tr} = 0.2$ for a sample with $\theta = 30°$ and $F_{tr} = 1.0$.

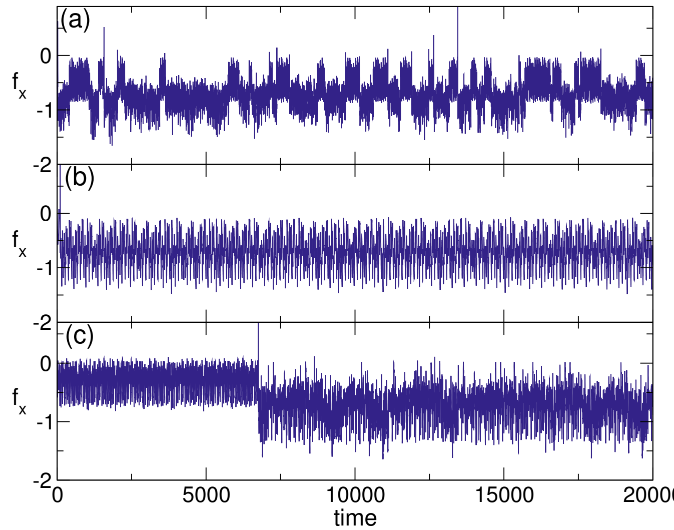

FIG. 13: (a) $f_x(t)$ for a sample with $\theta = 30°$ and $F_{tr} = 1.8$ at $v_{tr} = 0.12$ in phase IV. The time series has a telegraph noise characteristic in which the two values are produced when the trap alternates between dragging one (higher f_x) or two (lower f_x) vortices. (b) In phase V at $v_{tr} = 0.02$, the trap always captures two vortices and the telegraph noise is lost. (c) In phase IV at $v_{tr} = 0.048$, there is a transient signature when the trap initially drags one vortex but then captures a second vortex, producing a clearly visible jump in f_x.

There is no longer a peak in $P(f_x)$ at $f_x = 0$ since the trap always contains one vortex. We find a periodic signal in $f_x(t)$ containing both stick-slip features and additional smoother oscillations between pairs of force spikes. The force spike pairs arise when the trap captures a new vortex or drops a trapped vortex. Since a trap with $F_{tr} = 1.0$ is not strong enough to confine two vortices, every time the trap captures a vortex it sheds the previously captured vortex. The process of bringing a trapped vortex close to a pinned vortex, followed by capture of the pinned vortex, produces a peak in $P(f_x)$ at $f_x = -0.2$. The smooth oscillations occurring on a longer time scale correspond to the transport of a vortex between pinning sites by the trap, since at $\theta = 30°$ the trap passes over a pinning site in every other column of the pinning array. When the trap passes between two pinned vortices at a distance $a/2$, the trapped vortex must cross an energy barrier generated by the repulsive vortex-vortex forces, giving a second peak in $P(f_x)$ at $f_x = -0.4$. In Fig. 12(c,d) we show $f_x(t)$ and $P(f_x)$ for $v_{tr} = 0.05$ in phase III for the $\theta = 30°$ and $F_{tr} = 1.0$ system from Fig. 12(a,b). At this low trap velocity, the trapped vortex produces a larger perturbation of the surrounding vortices as it moves, resulting in the appearance of additional peaks in $P(f_x)$. The highest peak in $P(f_x)$ at $f_x = -0.2$ results when the strongly trapped vortex passes through a pinning site and pushes the pinned vortex out of its way without escaping from the trap.

In phase IV, illustrated for a sample with $\theta = 30°$ and $F_{tr} = 1.8$ at $v_{tr} = 0.12$ in Fig. 13(a), $f_x(t)$ shows a strong

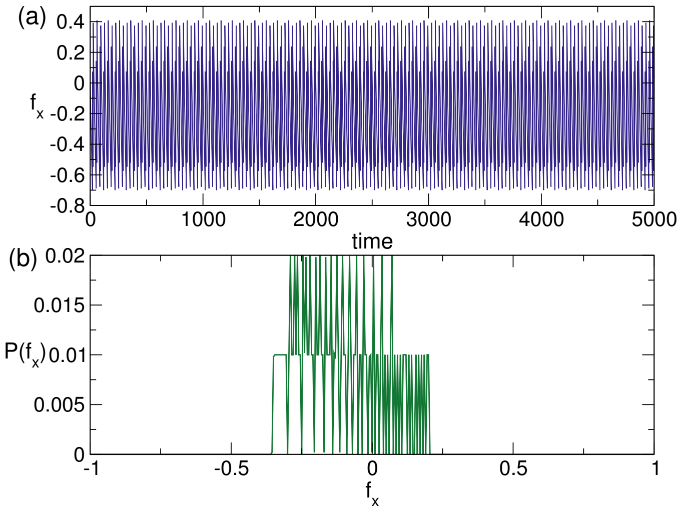

FIG. 14: (a) $f_x(t)$ in phase I for a sample with $\theta = 0^{\circ}$, $F_{tr} = 1.0$, and $v_{tr} = 0.3$. (b) The corresponding $P(f_x)$ indicates that the fluctuations are periodic.

telegraph noise signal in which two states arise when the trap alternates between dragging one or two vortices. In phase V at $v_{tr} = 0.02$, Fig. 13(b) indicates that the telegraph noise in $f_x(t)$ is lost since there are always two vortices in the trap, and the forces exerted on the trap are always in the negative x direction. Figure 13(c) shows a transient situation at $v_{tr} = 0.048$, where the trap is initially dragging one vortex but then captures a second vortex, as indicated by the drop in f_x to a more negative value.

In general, we find that when the trap is dragged along certain symmetry angles of the pinning array, such as $\theta = 0^{\circ}$ and $\theta = 45^{\circ}$, the force fluctuations contain a stronger periodic component, while for driving at incommensurate angles, the force fluctuations are more disordered. Previous work with particles driven over square pinning arrays showed that directional locking should occur at angles of $\theta = \tan^{-1}(n/m)$, where n and m are integers[62–66], so for driving at these locking angles, we expect the force fluctuations to be more periodic. In Fig. 14 we show $f_x(t)$ and $P(f_x)$ in phase I for a sample with $\theta = 0^{\circ}$ at $F_{tr} = 1.0$ and $v_{tr} = 0.3$. There is a strong periodic signal and $f_x(t)$ is much more ordered than the stick-slip time series shown in Fig. 11(a) for a $\theta = 30^{\circ}$ system in phase I at $F_{tr} = 1.0$ and $v_{tr} = 0.5$.

VI. DISCUSSION

Within the particle description we use, the number of vortices and their shape is held fixed; however, it is possible that a sufficiently strong trapping force could induce vortex shape distortions that could change the dynamics. Recent imaging experiments have shown how vortex dynamics can change when vortex distortion is taken into account beyond the London limit[67]. A similar breakdown of the particle model could also arise for other systems such as skyrmions dragged over different types of pinning substrates[68]. Additionally, if the trap is strong enough, then in the multiple vortex trapping phases IV and V, the trapped vortices may merge and form multiquantum states. Our results apply to the limit in which the trap is weak enough that such distortions do not occur. In experiments, it is likely that the tip speed will be in the limit of low v_{tr}; however, the phase diagrams of Fig. 6 indicate that most of the phases can be accessed even at the lowest trap velocities by varying the trap strength. We consider a two-dimensional system, but some three dimensional systems such as layered samples could produce different results due to additional three-dimensional effects such as the dissociation of vortices or line breaking effects.

Instead of employing a moving trap, it would also be possible to use a stationary trap of fixed strength and apply a current so that all of the vortices flow past the trap in order to exert forces on it. When the vortices are moving fast enough that the trap cannot capture a vortex, the system enters a decoupled state. We note that there are differences between the stationary and moving trap realizations. With the moving trap, the drive is local and applied only to the trap, whereas for the stationary trap, the current is applied to all of the vortices. A uniform current produces a constant force on the trapped vortex in the stationary trap rather than a constant relative velocity difference as in the case of the moving trap. One advantage of the stationary trap geometry is that it is not necessary to include a background pinning potential. Instead of using an applied current to drive vortices past the stationary trap, it is also possible to translate the vortices with dynamic pinning sites by means of sequential flashing of the pinning potential[69,70].

In this work we focus on a specific trap radius and vortex-vortex interaction strength, but we expect that the same dynamic phases should appear for a range of other parameters, such as at higher fields or different trap sizes, although the locations of the phase boundaries will likely shift to different trap strengths and velocities. Our results should also be robust for triangular rather than square pinning arrays; however, the high symmetry driving angles would be $\theta = 30^{\circ}$ and $\theta = 60^{\circ}$ for the triangular arrays instead of $\theta = 45^{\circ}$ for the square arrays. There is a slight energy difference between a square vortex lattice and a triangular vortex lattice, which may cause the phase transition boundaries to shift if a different pinning lattice symmetry is used. It could be also be interesting to consider the effects of dragging vortices with a trap over random, quasiperiodic, or anisotropic pinning arrays, but this is beyond the scope of the present work.

Our results should be general to other systems of particles interacting with periodic trap arrays, such as colloidal particles in optical or gravitational lattices, where the interactions between colloids can be of magnetic form with a $1/r^3$ behavior or of screened Coulomb or Yukawa form.

VII. SUMMARY

We have numerically examined vortex manipulation in superconductors with a periodic array of pinning sites by a local moving trap. We find five distinct phases depending on the trap strength and velocity. In phase I, which appears for low trap strength or large trap velocity, the vortices are decoupled from the trap, which can move a vortex within a pinning site but cannot depin it. The distribution of forces experienced by the trap has a peak at zero force corresponding to time intervals during which the trap is moving between adjacent pinning sites and contains no vortex. In the intermediate coupling phase II, the trap drags a vortex out of a pinning site and then exchanges that vortex with another vortex upon reaching the next occupied pinning site, so that the trap is always occupied by a vortex. In phase III, where intermediate trapping occurs, the trap can drag a single vortex over long distances, but still occasionally exchanges this vortex with another pinned vortex. Within phase III we find a counterintuitive effect in which the trap couples more strongly to a single vortex at higher velocities than at lower velocities, since at lower velocities there is enough time for a pinned vortex to complete an exchange with the trapped vortex. Phases II and III both exhibit stick-slip fluctuations of the force experienced by the trap that correlate with vortex exchange events and with the entry and exit of vortices from the trap. Phase IV is an intermittent multiple trapping regime in which the trap alternates between capturing one or two vortices, producing a telegraph noise signature in the trap force fluctuation signal. In phase V, where the trap is strongly coupled and always captures two vortices, the telegraph noise signal is lost. We map the evolutions of these phases for varied trap coupling strength, trap velocity, and the angle of trap motion with respect to the x symmetry axis of the pinning array. For a given trap coupling force, transitions among the phases occur as a function of increasing trap velocity. Our results should be general to other types of particle systems with a periodic substrate subjected to a moving local trap, such as colloidal particles, skyrmions, or ions on optical traps.

Acknowledgments

This work was carried out under the auspices of the NNSA of the U.S. DoE at LANL under Contract No. DE-AC52-06NA25396.

[1] M. Baert, V.V. Metlushko, R. Jonckheere, V.V. Moshchalkov, and Y. Bruynseraede, Composite flux-line lattices stabilized in superconducting films by a regular array of artificial defects, Phys. Rev. Lett. **74**, 3269 (1995).

[2] C. Reichhardt, C.J. Olson, and F. Nori, Commensurate and incommensurate vortex states in superconductors with periodic pinning arrays, Phys. Rev. B **57**, 7937 (1998).

[3] G.R. Berdiyorov, M.V. Milosevic, and F.M. Peeters, Novel commensurability effects in superconducting films with antidot arrays, Phys. Rev. Lett. **96**, 207001 (2006).

[4] M. Vélez, J.I. Martín, J.E. Villegas, A. Hoffmann, E.M. González, J.L. Vicent, and I.K. Schuller, Superconducting vortex pinning with artificial magnetic nanostructures, J. Magn. Magn. Mater. **320**, 2547 (2008).

[5] I.A. Sadovskyy, Y.L. Wang, Z.-L. Xiao, W.-K. Kwok, and A. Glatz, Effect of hexagonal patterned arrays and defect geometry on the critical current of superconducting films, Phys. Rev. B **95**, 075303 (2017).

[6] B. Gränz, S.E. Korshunov, V.B. Geshkenbein, and G. Blatter, Competing structures in two dimensions: Square-to-hexagonal transition, Phys. Rev. B 94, 054110 (2016).

[7] D. S. Fisher, Collective transport in random media: From superconductors to earthquakes, Phys. Rep. **301**, 113 (1998).

[8] J. Gutierrez, A.V. Silhanek, J. Van de Vondel, W. Gillijns, and V.V. Moshchalkov, Transition from turbulent to nearly laminar vortex flow in superconductors with periodic pinning, Phys. Rev. B **80**, 140514(R) (2009).

[9] S. Avci, Z.L. Xiao, J. Hua, A. Imre, R. Divan, J. Pearson, U. Welp, W.K. Kwok, and G.W. Crabtree, Matching effect and dynamic phases of vortex matter in $Bi_2Sr_2CaCu_2O_8$ nanoribbon with a periodic array of holes, Appl. Phys. Lett. **97**, 042511 (2010).

[10] N. Poccia, T.I. Baturina, F. Coneri, C.G. Molenaar, X.R. Wang, G. Bianconi, A. Brinkman, H. Hilgenkamp, A.A. Golubov, and V.M. Vinokur, Critical behavior at a dynamic vortex insulator-to-metal transition, Science **349**, 1202 (2015).

[11] C. Reichhardt and C. J. Olson Reichhardt, Depinning and nonequilibrium dynamic phases of particle assemblies driven over random and ordered substrates: A review, Rep. Prog. Phys. **80**, 026501 (2017).

[12] G. Blatter, M. V. Feigel'man, V.B. Geshkenbein, A.I. Larkin, and V.M. Vinokur, Vortices in high-temperature superconductors. Rev. Mod. Phys. **66**, 1125 (1994).

[13] T. Giamarchi and P. Le Doussal, Phase diagrams of flux lattices with disorder, Phys. Rev. B **55**, 6577 (1997).

[14] I. Guillamón, R. Córdoba, J. Sesé, J.M. De Teresa, M.R. Ibarra, S. Viera, and H. Suderow, Enhancement of long-range correlations in a 2D vortex lattice by an incommensurate 1D disorder potential, Nature Phys. **10**, 851 (2014).

[15] W.K. Kwok, U. Welp, A. Glatz, A.E. Koshelev, K.J. Kihlstrom, and G.W. Crabtree, Vortices in high-performance high-temperature superconductors, Rep. Prog. Phys. **79**, 116501 (2016).

[16] C.J.O. Reichhardt and M.B. Hastings, Do Vortices Entangle? Phys. Rev. Lett. **92**, 157002 (2004).

[17] Y. Kafri, D. Nelson, and A. Polkovnikov, Unzipping vortices in type-II superconductors, Phys. Rev. B **76**, 144501 (2007).

[18] M.B. Hastings, C.J.O. Reichhardt, and C. Reichhardt, Ratchet cellular automata, Phys. Rev. Lett. **90**, 247004 (2003).

[19] M.V. Milosevic, G.R. Berdiyorov, and F.M. Peeters, Flux-

onic cellular automata, Appl. Phys. Lett. **91**, 212501 (2007).
[20] M.V. Milosevic, A. Kanda, S. Hatsumi, F. M. Peeters, and Y. Ootuka, Local current injection into mesoscopic superconductors for the manipulation of quantum states, Phys. Rev. Lett. **103**, 217003 (2009).
[21] T. Golod, A. Iovan, and V. M. Krasnov, Single Abrikosov vortices as quantized information bits, Nat. Commun. **6**, 8628 (2015).
[22] D.A. Ivanov, Non-Abelian statistics of half-quantum vortices in p-wave superconductors, Phys. Rev. Lett. **86**, 268 (2001).
[23] H.-H. Sun *et al.*, Majorana zero mode detected with spin selective Andreev reflection in the vortex of a topological superconductor, Phys. Rev. Lett. **116**, 257003 (2016).
[24] H.-H. Sun and J.-F. Jia, Detection of Majorana zero mode in the vortex, npj Quantum Materials **2**, 34 (2017).
[25] Q.-F. Liang, Z. Wang, and X. Hu, Manipulation of Majorana fermions by point-like gate voltage in the vortex state of a topological superconductor, EPL **99**, 50004 (2012).
[26] H.-D. Wu and T. Zhou, Vortex pinning by the point potential in topological superconductors: a scheme for braiding Majorana bound states, Phys. Rev. B **96**, 184508 (2017).
[27] B.W. Gardner, J.C. Wynn, D.A. Bonn, R. Liang, W.N. Hardy, J.R. Kirtley, V.G. Kogan, and K.A. Moler, Manipulation of single vortices in $YBa_2Cu_3O_{6.354}$ with a locally applied magnetic field, Appl. Phys. Lett. **80**, 1010 (2002).
[28] E.W.J. Straver, J.E. Hoffman, O.M. Auslaender, D. Rugar, and K.A. Moler, Controlled manipulation of individual vortices in a superconductor, Appl. Phys. Lett. **93**, 172514 (2008).
[29] C. Reichhardt, High-temperature superconductors: Vortices wiggled and dragged, Nature Phys. **5**, 15 (2009).
[30] O.M. Auslaender, L. Luan, E.W.J. Straver, J.E. Hoffman, N.C. Koshnick, E. Zeldov, D.A. Bonn, R. Liang, W.N. Hardy, and K.A. Moler, Mechanics of individual isolated vortices in a cuprate superconductor, Nature Phys. **5**, 35 (2009).
[31] L. Luan, O.M. Auslaender, D.A. Bonn, R. Liang, W.N. Hardy, and K.A. Moler, Magnetic force microscopy study of interlayer kinks in individual vortices in the underdoped cuprate superconductor $YBa_2Cu_3O_{6+x}$, Phys. Rev. B **79**, 214530 (2009).
[32] N. Shapira, Y. Lamhot, O. Shpielberg, Y. Kafri, B. J. Ramshaw, D.A. Bonn, R. Liang, W.N. Hardy, and O.M. Auslaender, Disorder-induced power-law response of a superconducting vortex on a plane, Phys. Rev. B **92**, 100501(R) (2015).
[33] I.S. Veshchunov, W. Magrini, S.V. Mironov, A.G. Godin, J.-B. Trebbia, A.I. Buzdin, Ph. Tamarat, and B. Lounis, Optical manipulation of single flux quanta, Nature Commun. **7**, 12801 (2016).
[34] A. Kremen, S. Wissberg, N. Haham, E. Persky, Y. Frenkel, and B. Kalisky, Mechanical control of individual superconducting vortices, Nano Lett. **16**, 1626 (2016).
[35] A. Crassous, R. Bernard, S. Fusil, K. Bouzehouane, D. Le Bourdais, S. Enouz-Vedrenne, J. Briatico, M. Bibes, A. Barthélémy, and J.E. Villegas, Nanoscale electrostatic manipulation of magnetic flux quanta in ferroelectric/superconductor $BiFeO_3/YBa_2Cu_3O_7$ heterostructures, Phys. Rev. Lett. **107**, 247002 (2011).
[36] L. Embon, Y. Anahory, A. Suhov, D. Halbertal, J. Cuppens, A. Yakovenko, A. Uri, Y. Myasoedov, M. L. Rappaport, M. E. Huber, A. Gurevich, and E. Zeldov, Probing dynamics and pinning of single vortices in superconductors at nanometer scales, Sci. Rep. **5**, 7598 (2015).
[37] J.-Y. Ge, V.N. Gladilin, J. Tempere, C. Xue, J.T. Devreese, J. Van de Vondel, Y. Zhou, and V.V. Moshchalkov, Nanoscale assembly of superconducting vortices with scanning tunnelling microscope tip, Nature Commun. **7**, 13880 (2016).
[38] J.-Y. Ge, V.N. Gladilin, J. Tempere, J. Devreese, and V.V. Moshchalkov, Controlled generation of quantized vortex-antivortex pairs in a superconducting condensate, Nano Lett. **17**, 5003 (2017).
[39] M.B. Hastings, C.J.O. Reichhardt, and C. Reichhardt, Depinning by fracture in a glassy background, Phys. Rev. Lett. **90**, 098302 (2003).
[40] P. Habdas, D. Schaar, A.C. Levitt, and E.R. Weeks, Forced motion of a probe particle near the colloidal glass transition, Europhys. Lett. **67**, 477 (2004).
[41] C.J.O. Reichhardt and C. Reichhardt, Viscous decoupling transitions for individually dragged particles in systems with quenched disorder, Phys. Rev. E **78**, 011402 (2008).
[42] D. Winter, J. Horbach, P. Virnau, and K. Binder, Active nonlinear microrheology in a glass-forming Yukawa fluid, Phys. Rev. Lett. **108**, 028303 (2012).
[43] Th. Voigtmann and M. Fuchs, Force-driven microrheology, Eur. Phys. J. Spec. Top. **222**, 2819 (2013).
[44] C. Reichhardt and C.J.O. Reichhardt, Local melting and drag for a particle driven through a colloidal crystal, Phys. Rev. Lett. **92**, 108301 (2004).
[45] R.P.A. Dullens and C. Bechinger, Shear thinning and local melting of colloidal crystals, Phys. Rev. Lett. **107**, 138301 (2011).
[46] K. Harada, O. Kamimura, H. Kasai, T. Matsuda, A. Tonomura, and V.V. Moshchalkov, Direct observation of vortex dynamics in superconducting films with regular arrays of defects, Science **274**, 1167 (1996).
[47] S. Tung, V. Schweikhard, and E.A. Cornell, Observation of vortex pinning in Bose-Einstein condensates, Phys. Rev. Lett. **97**, 240402 (2006).
[48] C. Reichhardt, D. Ray, and C.J.O. Reichhardt, Quantized transport for a skyrmion moving on a two-dimensional periodic substrate, Phys. Rev. B **91**, 104426 (2015).
[49] A. Benassi, A. Vanossi, and E. Tosatti, Nanofriction in cold ion traps, Nature Commun. **2**, 236 (2011).
[50] P.T. Korda, M.B. Taylor, and D.G. Grier, Kinetically locked-In colloidal transport in an array of optical tweezers, Phys. Rev. Lett. **89**, 128301 (2002).
[51] T. Bohlein, J. Mikhael, and C. Bechinger, Observation of kinks and antikinks in colloidal monolayers driven across ordered surfaces, Nature Mater. **11**, 126 (2012).
[52] A. Vanossi, N. Manini, and E. Tosatti, Static and dynamic friction in sliding colloidal monolayers, Proc. Natl. Acad. Sci. (U.S.A.) **109**, 16429 (2012).
[53] A. Vanossi, N. Manini, M. Urbakh, S. Zapperi, and E. Tosatti, Modeling friction: From nanoscale to mesoscale, Rev. Mod. Phys. **85**, 529 (2013).
[54] R. Willa, A.E. Koshelev, I.A. Sadovskyy, and A. Glatz, Strong-pinning regimes by spherical inclusions in anisotropic type-II superconductors, Supercond. Sci. Technol. **31**, 014001 (2018).
[55] C. Reichhardt, C. J. Olson, and F. Nori, Nonequilibrium dynamic phases and plastic flow of driven vortex lattices in superconductors with periodic arrays of pinning sites, Phys. Rev. B **58**, 6534 (1998).
[56] V. Misko, S. Savelev, A. Rakhmanov, and F. Nori, Nega-

tive differential resistivity in superconductors with periodic arrays of pinning sites, Phys. Rev. B **75**, 024509 (2007).

[57] G. Blatter, V.B. Geshkenbein, and J.A.G. Koopmann, Weak to strong pinning crossover, Phys. Rev. Lett. **92**, 067009 (2004).

[58] L.N. Bulaevskii and S.Z. Lin, Prediction of polaronlike vortices and a dissociation depinning transition in magnetic superconductors: the example of $ErNi_2B_2C$, Phys. Rev. Lett. **109**, 027001 (2012).

[59] S.-Z. Lin and C. Reichhardt, Stabilizing fractional vortices in multiband superconductors with periodic pinning arrays, Phys. Rev. B **87**, 100508(R) (2013).

[60] S. Scheidl and V.M. Vinokur, Dynamic melting and decoupling of the vortex lattice in layered superconductors, Phys.l Rev. B **57**, 13800 (1998).

[61] A. Sheikhzada and A. Gurevich, Dynamic transition of vortices into phase slips and generation of vortex-antivortex pairs in thin film Josephson junctions under dc and ac currents, Phys. Rev. B **95**, 214507 (2017).

[62] C. Reichhardt and F. Nori, Phase locking, devil's staircases, Farey trees, and Arnold tongues in driven vortex lattices with periodic pinning, Phys. Rev. Lett. **82**, 414 (1999).

[63] J. M. Sancho, M. Khoury, K. Lindenberg, and A. M. Lacasta, Particle separation by external fields on periodic surfaces, J. Phys.: Condens. Matter **17**, S4151 (2005).

[64] J. Villegas, E. Gonzalez, M. Montero, I. Schuller, and J. Vicent, Vortex-lattice dynamics with channeled pinning potential landscapes, Phys. Rev. B **72**, 064507 (2005).

[65] J. Koplik and G. Drazer, Nanoscale simulations of directional locking, Phys. Fluids **22**, 052005 (2010).

[66] C. Reichhardt and C. J. O. Reichhardt, Structural transitions and dynamical regimes for directional locking of vortices and colloids driven over periodic substrates, J. Phys.: Condens. Matter **24**, 225702 (2012).

[67] L. Embon, Y. Anahory, Z.L. Jelic, E.O. Lachman, Y. Myasoedov, M.E. Huber, G.P. Mikitik, A.V. Silhanek, M.V. Milosevic, A. Gurevich, and E. Zeldov, Imaging of superfast dynamics and flow instabilities of superconducting vortices, Nat. Commun. **8**, 85 (2017).

[68] D. Stosic, T.B. Ludermir, and M.V. Milosevic, Pinning of magnetic skyrmions in a monolayer Co film on Pt(111): Theoretical characterization and exemplified utilization, Phys. Rev. B **96**, 214403 (2017).

[69] Z.L. Jelic, M.V. Milosevic, J. Van de Vondel, and A.V. Silhanek, Stroboscopic phenomena in superconductors with dynamic pinning landscape, Sci. Rep. **5**, 14604 (2015).

[70] Z.L. Jelic, M.V. Milosevic, and A.V. Silhanek, Velocimetry of superconducting vortices based on stroboscopic resonances, Sci. Rep. **6**, 35687 (2016).